

## Frequency as the *Greenest* Additive for Metal Plating: Mathematical and Experimental Study of Forcing Voltage Effects on Electrochemical Growth Dynamics

Benedetto Bozzini<sup>1,\*</sup>, Deborah Lacitignola<sup>2</sup>, Ivonne Sgura<sup>3</sup>

<sup>1</sup> Dipartimento di Ingegneria dell'Innovazione- Università del Salento, Via per Monteroni – 73100 Lecce, Italy.

<sup>2</sup> Dipartimento di Scienze Motorie e della Salute – Università di Cassino, Campus Folcara – 03043 Cassino, Italy.

<sup>3</sup> Dipartimento di Matematica “E. De Giorgi” - Università del Salento, Via per Arnesano – 73100 Lecce, Italy.

\*E-mail: [benedetto.bozzini@unisalento.it](mailto:benedetto.bozzini@unisalento.it)

Received: 31 March 2011 / Accepted: 6 September 2011 / Published: 1 October 2011

---

Metal plating is a well-assessed and widespread technology. Though being a mature process (Ag plating is in fact the first known application of Volta's battery in 1801, Al electrolysis was used to fabricate Napoleon III's tableware for very special occasions at the imperial French court, present-day decorative- and hard- Cr electrodeposition thrive on a patent dating back to 1860), its successful implementation in many cutting-edge technologies seems the only viable approach to certain material fabrication issues, especially in the nanoscale (e.g. state-of-the-art and next-generation ULSI technologies). Curiously, in most cases, industrial success of this class of processes is achieved at the cost of using extremely toxic and polluting additives. This is essentially due to the poor fundamental knowledge of the physico-chemical basis of electrochemical metal growth and, in particular, of its dynamics. In this study we wish to highlight, from both the mathematical and the experimental points of view, the fact that - owing to the peculiarities of the coupled morphological and chemical dynamic processes going on at the electrochemical interface during metal plating at controlled potential - the application of a small sinusoidal forcing term is able to drive the morphology of the growing film towards the industrially desirable surface finish in the way currently achieved only by non-green additives.

---

**Keywords:** Electrodeposition; Pattern Formation; Numerical Simulations

### 1. INTRODUCTION

Metal electroplating is ubiquitous in surface treatment technologies and has wide-ranging applications from biomedical to electronics and from energy production and conversion to aerospace.

Unfortunately - notwithstanding many academic and industrial efforts to improve both products and process chemistries - electroplating can be regarded as one of the most polluting industries. Apart from the plating of intrinsically environmentally unfriendly metals, such as: Cd, Cr and Ni, essentially all industrially viable processes for the electrodeposition of non-toxic metals, such as: Ag, Au and Zn, contain extremely poisonous additives, some among which are also able to attract the worried attention of the general public, exposed to famous crime novels, such as: arsenic (for bright gold), strichnin (for nickel free of pinholes) and cyanide (for gold, silver, copper, zinc and cadmium). The authors of this paper have been active for a long time in both fundamental and applied studies of additives for metal plating and wish to communicate a novel approach that may help in the effort of getting rid of obnoxious metal plating additives by judicious use of the electrical variables, playing in this case the role of an additive that can be regarded as green indeed. In particular, we have found that - during potentiostatic (constant applied electrodic potential, the single most common industrial situation) plating, superposition of a small sinusoidal perturbation can yield notable levelling effects. It is immediately worth stressing the utter difference between the dynamic approach we are proposing in this research with respect to traditional pulse plating. Pulse plating is based on sequences of potential or current rectangles, aiming at an improved control of mass transport at the electrode, in turn giving rise to some degree of levelling (e.g. [1] and references therein contained). Our approach, instead, is based on some peculiarities of the coupling of morphological and surface chemical dynamics - that we have highlighted in a series of recent papers [2—6] - that allow for control of the 3D electrocrystallisation process. Such dynamics exhibits some subtle interactions with an applied forcing frequency, giving rise to intriguing effects that are likely to have a bearing on the development of green metal plating chemistries.

## 2. A MATHEMATICAL MODEL FOR ELECTRO-PLATING

The modelling basis for our idea of applying an electrochemical forcing term is an extension to the electrochemical realm of a class of continuum models (CM) originally devised for crystal growth by Molecular Beam Epitaxy (MBE), giving a theoretical description of such processes on lengthscales ranging from some tens of atomic distances to a few microns. An accurate presentation of the mathematical background can be found in [7, 8]. At variance with the conventional literature approach to CM, we are also coupling surface chemistry to the profile dynamics. In this approach, we describe the evolution of the electrodeposit surface profile obtained as the solution of a balance equation. The flow terms describe inflow and outflow of material contributing to the build-up of the morphology, while the source terms account for generation (deposition) and loss (corrosion, desorption) of the relevant material. CMs of this type can be regarded as an acceptable description of profile dynamics, provided certain conditions on length and timescales are defined, that are summarised in the Appendix. Apart from the original electrochemical source term, the equation for the proposed morphological dynamics is based on Villain's pseudo-diffusion model [8]. In the absence of desorption, at sufficiently low temperatures, diffusion of adatoms is anisotropic on long lengthscales, because it is biased by reflections against terrace edges; if the Schwobel effect is operative, such reflecting edges are

downwards-steps. By a polynomial expansion approach, the mathematical model studied in [3—6] exhibited a surprisingly rich phenomenology (e.g. the initiation of spatial patterns induced by diffusion and the existence of travelling wave solutions) and was able to capture the essential features of pattern development observed in experiments. Here we present the effect of a periodic external forcing both on the impact of roughness in electrodeposition experiments and on the Turing patterns found in [5]. For compactness of presentation, we briefly derive the model with a forcing, on the basis of the original model fully explained in [5]. We consider one chemical species - modelling an additive able to control morphology, such as, e.g., a leveller - adsorbed at the surface of the growing cathode, so that we deal with a system of two reaction-diffusion equations, one for the morphology and one for the chemistry. The equation for the morphological dynamics in the presence of external periodic forcing is given by:

$$\frac{\partial \eta}{\partial \tau} = D_s^* \Delta \eta + S^* + S_{forc}^*, \quad \text{with} \quad S^* = \alpha \frac{\eta^2}{1 + \eta} - \beta \eta \theta, \quad (1)$$

where  $\Delta = \frac{\partial^2}{\partial x^2} + \frac{\partial^2}{\partial y^2}$ . Here  $\eta(x, y, \tau)$  is the dimensionless electrode shape (i.e. the dimensionless intersection of the electrodeposit surface with a plane normal to the substrate),  $x$  and  $y$  are the dimensionless space coordinates,  $\tau$  is the dimensionless time and  $D_s^*$  is the dimensionless surface diffusion coefficient of adatoms. In the source term  $S^*$ ,  $\theta(x, y, \tau)$  is the surface coverage with the adsorbed chemical species, the parameters  $\alpha$  and  $\beta$  are strictly positive and weight the two terms in  $S^*$  accounting for: (i) localization of the ECD process and (ii) effects on the ECD rate of the presence of adsorbates, respectively. The term  $S_{forc}^*$  instead accounts for the presence of the periodic external forcing which is here assumed to be sinusoidal.

The presence of adsorbable species in the ECD bath gives rise to the fact that  $\theta(x, y, \tau)$  develops at a growing electrochemical interface as a function of space and time, as well as to the nature of the adsorbable species and of the surface active sites. The surface coverage dynamics can be described, as customary in chemical kinetics, in terms of a material balance with a source term containing positive and negative contributions related to adsorption and desorption. More precisely, the dimensionless form for the surface chemical dynamics can be expressed as:

$$\frac{\partial \theta}{\partial \tau} = D_{sc}^* \Delta \theta + S_c^*, \quad (2)$$

where  $D_{sc}^*$  is the surface diffusion coefficient of the additive and  $S_c^*$  is the chemical source term given by

$$S_c^* = K_{ADS}^* (\eta, \theta)(1 - \theta) - K_{DES}^* (\eta, \theta)\theta,$$

where  $K_{ADS}^*$  and  $K_{DES}^*$  represent the adsorption and desorption rate constants, respectively.

By coupling equations (1) and (2), and by defining

$$t = D_s^* \tau, \quad d = \frac{D_{sc}^*}{D_s^*}, \quad \sigma = \frac{1}{D_s^*}, \quad \rho = \frac{\beta}{D_s^*}$$

one obtains the following model in dimensionless form:

$$\begin{cases} \frac{\partial \eta}{\partial t} = \Delta \eta + \rho(f(\eta, \theta) + F(t)), \\ \frac{\partial \theta}{\partial t} = d \Delta \theta + \sigma g(\eta, \theta) \end{cases} \quad (3)$$

$$f(\eta, \theta) = \frac{\varepsilon \eta^2}{1 + \eta} - \eta \theta, \quad g(\eta, \theta) = K_{ADS}^*(\eta, \theta) - [K_{ADS}^*(\eta, \theta) + K_{DES}^*(\eta, \theta)] \theta, \quad (4)$$

where  $\varepsilon = \frac{\alpha}{\beta}$ , and the forcing term is specialised as

$$F(t) = \tilde{A} \sin(\omega t) \quad (5)$$

where  $\tilde{A} = K A_0$  and  $\omega$  are dimensionless. The parameter  $K [V^{-1}]$  is a constant assembling the electrokinetic Butler-Volmer parameters in the form:

$$K = 2i_0 \times a \times n, \quad (6)$$

where  $i_0 [Am^{-2}]$  is the exchange current density,  $a$  (adimensional) is the anodic and cathodic Tafel slope,  $n [m^2 A^{-1} V^{-1}]$  is a normalization factor. The term  $A_0 [V]$  represents the forcing amplitude and  $\omega$  represents the adimensional forcing frequency, such that  $\omega = \omega_{exp} [Hz] \cdot T_{exp} [sec]$ ,  $\omega_{exp}$  is the experimental frequency imposed,  $T_{exp}$  is a representative time for electrodeposition.

Since typically, adsorption and desorption are controlled by electrochemical conditions, it is possible to express the respective rates in Eq. (4) as [9]

$$K_{ADS}^* = A \exp(a\eta + b\theta), \quad K_{DES}^* = A_1 \cdot \exp(a_1\eta + b_1\theta) \quad (7)$$

where  $A, A_1, a, a_1, b, b_1$  are positive parameters. These expressions essentially amount to the linearisation of an activation energy term, depending on both electrode potential and surface chemistry, thus accounting for electrocapillary effects as well as lateral interaction among adsorbates.

The reaction-diffusion system (3) is defined for  $(x, y, t) \in \Omega \times [0, T]$  with  $\Omega = [0, L_1] \times [0, L_2]$  and  $L_1, L_2$  characteristic lengths of the electrode,  $T$  a characteristic time of the electrodeposition process. We also require (3) to be equipped with zero-flux boundary conditions and the following initial conditions at time  $t=0$ :

$$\eta(x,y,0) = \eta_0(x,y) \quad \text{and} \quad \theta(x,y,0) = \theta_0(x,y), \quad (x,y) \in \Omega$$

### 2.1. Morphological pattern formation

Chiefly motivated by the technological requirement of obtaining smooth metallic films, we concentrate on the influence of the periodic driving force in pattern suppression, the modelling correlate of smoothing in practical metal plating. For this reason, we study the effect of the periodic external forcing on the solutions of model (3)-(5). The unforced case - obtained by setting  $F(t) = 0$  in (3) - has been insightfully analysed in [5], where the existence of Turing spatial patterns has been shown through the destabilisation of the spatially uniform steady state. The mathematical analysis has been performed by considering some constraints on the parameters of the model and a set of conditions on them has in fact been obtained, ensuring the initiation of spatial patterns. In particular, the diffusion parameter  $d$  has been shown to be essential for the arising of instability and the appearance of spatial patterns. With regard to pattern selection, the peculiar role of the parameter  $a$  has been stressed, representing the inverse of the energy barrier that has to be overcome by electrons tunneling from the electrode into the electrolyte to reduce metal adatom precursors (e.g. [10]). A detailed discussion on these points is provided in the Appendix.

In two space dimensions, the most typical patterns for Turing systems turn out to be stripes - corresponding to the formation of ridges of correlated crystallites in electrodeposits - or exagonally arranged spots - corresponding to the outgrowth of isolated crystallites in actual metal film plating -, even if in some cases different types have been observed as rhombic or labyrinthine patterns [11]. To predict the spatial characteristics of the resulting patterns, linear analysis is not enough, since pattern selection is governed by complicated nonlinear dynamics. To this aim, theoretical investigations must rely on nonlinear bifurcation analysis and on the use of the amplitude equations formalism, see i.e [12—15]. For this reason, we approach the pattern selection problem numerically, focussing on the following morphological features of the patterns: (i) stationary pattern type, i.e. *spots* or *spots and worms*; (ii) transient pattern type.

Setting the diffusion parameter  $d$  near the threshold value  $d_c$  responsible for pattern initiation and by properly varying the parameter  $a$ , two different types of patterns - actually encountered in experiments - are qualitatively reproduced as stationary Turing patterns. On the other hand, for representative values of the parameter  $a$ , interesting transient patterns can arise, able to account for several observed morphological peculiarities, such as the presence of holes in films [5]. As far as the feature (i) is concerned, we find that very low values of  $a$ , i.e.  $a = a_{min}$ , lead to a stationary Turing pattern in which coexistence between spots and worms is clearly established [5]. By increasing the value of  $a$  up to  $a_{max}$ , only spots survive. This kind of phenomenology corresponds to the relevant physical chemistry in a straightforward way. In fact, relatively high  $a$  values correspond (under otherwise identical chemical and polarisation conditions) to a high surface density of adatoms, ending up incorporated into high-energy sites and thereby causing unstable growth, eventually yielding isolated outgrowth features, such as: stalks, dendrites or piles of spheroidal crystallites, according to the specific system [16,17]. Such outgrowth features, viewed in plane, would correspond to a pattern

of isolated spots [5]. To the contrary, relatively low  $a$  values correspond to the possibility for adatoms to reach low-energy crystal sites, where they contribute to the formation of more correlated morphologies, such as terraces and islands, tending to outgrow into ridges. On the other hand, fixing  $a=a_{min}$ , the effect of increasing  $d$  from  $d_c$ , is to obtain only spots at the stationary pattern. To explore how the presence of an external driving force can affect the morphological features of the above-discussed patterns, we consider the model given by Eqs. (3)-(5) with the periodic forcing term  $F(t)$  of Eq. (5).

### 3. NUMERICAL STUDY OF THE IMPACT OF FREQUENCY ON MORPHOLOGY

In the adimensional model (3), the only forced equation is the first one for the morphology  $\eta(x,y,t)$ . For our study, we consider the forcing term in Eq.(5) with a fixed amplitude  $\tilde{A}=K A_0$  and variable frequency  $\omega$ . In particular, by fixing  $i_0 = 1[Am^{-2}]$  the exchange current density and  $n = 0.98 [m^2A^{-1}V^{-1}]$  the normalization factor, by Eq.(6)  $K = 1.76 [V^{-1}]$  holds. Moreover, the fixed amplitude for the sinusoid is given by  $A_0 = 0.01 [V]$ . The (adimensional) frequency  $\omega$  will be varied in the range  $0 \leq \omega \leq \omega_f$ . Recall in fact that  $\omega = \omega_{exp}[Hz] \cdot 100[sec]$ , and the range  $\omega_{exp} \in [10^{-3}, 10^5]Hz$  is obtained for experimental considerations that can be easily derived with common electrochemical instrumentation.

In the dynamics, a key role is played by the equilibria obtained in correspondence of the maximum and the minimum of the imposed sinusoid, that is  $F(t)= \pm \tilde{A}$ , where according to the above-reported discussion, a fixed value is chosen as:  $\tilde{A}=K \cdot A_0 = 1.76 \cdot 0.01= 0.0176$  ( $[K]=1/V, [A_0]=V$ ). With this choice, three equilibria exist as real zeros of the equations

$$f(\eta, \theta) + \tilde{A} = 0 \quad g(\eta, \theta) = 0,$$

which are given by  $E_1^+ = (\eta_1^+, \theta_1^+)$ ,  $E_2^+ = (\eta_2^+, \theta_2^+)$ ,  $E_3^+ = (\eta_3^+, \theta_3^+)$ , whereas one equilibrium may be found as real zero of the equations

$$f(\eta, \theta) - \tilde{A} = 0 \quad g(\eta, \theta) = 0,$$

that is  $E_1^- = (\eta_1^-, \theta_1^-)$ . By using the classical stability method for nonlinear dynamical systems, we get insight on the stability properties of such equilibria:  $E_1^+$  is a stable node;  $E_2^+$  is a saddle;  $E_3^+$  is a stable focus and  $E_1^-$  is a stable node. For our purpose, only the stable equilibria have a relevant role for the scenarios in the time-dependent regimes. We decide to discuss the scenarios regarding only the morphology, that is the  $\eta$ 's values of the relevant equilibria  $E_1^-, E_1^+, E_3^+$ . Hence, our study will investigate the behaviours of model solutions when the frequency  $\omega$  varies in a range corresponding to classical experimental situations. The other parameters of the model are fixed in correspondence of the worst morphological instability situation of the unforced case [5], namely we focus on spatial patterns

exhibiting only spots. The related parameter values are given in the Appendix, in particular  $a=0.9$  holds.

For the chosen parameter values and for the above value of the amplitude  $\tilde{A}$ , the numerical values of the three equilibria  $E_1^+$ ,  $E_2^+$ ,  $E_3^+$  are given by:

$$E_1^+ = (0.1132, 0.2063), E_2^+ = (0.8655, 0.2523), E_3^+ = (2.2812, 0.3553)$$

The numerical value of  $E_1^-$  is instead:

$$E_1^- = (-0.0745, 0.1958).$$

To solve the forced reaction-diffusion system on the rectangular spatial domain for the time  $t \in [0, T]$ , we employ the Comsol Multiphysics package [18], based on the finite element method in space. Numerical simulations, have been performed in the domain  $\Omega = [0, 100] \times [0, 70]$ , by considering a spatially distributed random infinitesimal perturbation around the non-trivial stationary unforced equilibrium  $E_2 = (\eta_e, \theta_e) = (2, 1/3)$  as starting surface profiles for the time evolution.

To achieve accurate simulations both in space and time, able to capture the main features of the expected spatial patterns, we use a sufficiently fine mesh (almost 35000 degrees of freedom) and we select as time integrator the BDF (implicit) schemes of high order (up to five), with variable stepsize. Moreover, in order to obtain accurate results, time steps less than  $h_t \cong 1/\omega$  could be used. It is worth noting that, since we are interested in tracking and check long time *asymptotic* behaviour of the oscillatory solutions, this choice could imply sometimes time-consuming runs of the program (especially for high frequency values), even if iterative methods and preconditioning techniques are used to solve the linear systems involved. In our simulations, we use a variable stepsize strategy in time, such that  $h_t \leq 0.01$ . The numerical results obtained by our simulations for long-time approximations identify four qualitatively different “asymptotic” scenarios, corresponding to four ranges of frequency  $\omega$ . We classify them as follows:

**(A)** - low-frequency scenario  $0 \leq \omega \leq \omega_A$ : *only spots*;

**(B)** - lower intermediate frequency scenario  $\omega_A \leq \omega \leq \omega^*$ : *smooth* nearly-homogeneous surface.

In this case the “asymptotic” solution oscillates between the two spatially homogeneous values  $\eta_1^-$  and  $\eta_1^+$

**(C)** - upper intermediate frequency scenario  $\omega^* < \omega < \omega_C$ : *beat* or pulsating spots

**(D)** - high-frequency scenario  $\omega_C \leq \omega \leq \omega_D$ : *only spots* as in (A).

In Fig.1 these qualitative scenarios are shown for the morphology solutions  $\eta(x, y, T)$  at the “asymptotic” time  $T$ .

As already observed in [5], the actual morphologies found in electrodeposited metal samples, typically do not correspond to asymptotic conditions, but rather to transients interrupted after a given electroplating time, ideally corresponding to the target film thickness, has been reached. For this reason, it is interesting to investigate also the types of morphological behaviour developing during the transients. In all cases, the numerical solution moves away from the initial condition and the following

transient behaviours are observed, evolving towards one of the four asymptotic scenarios described above.

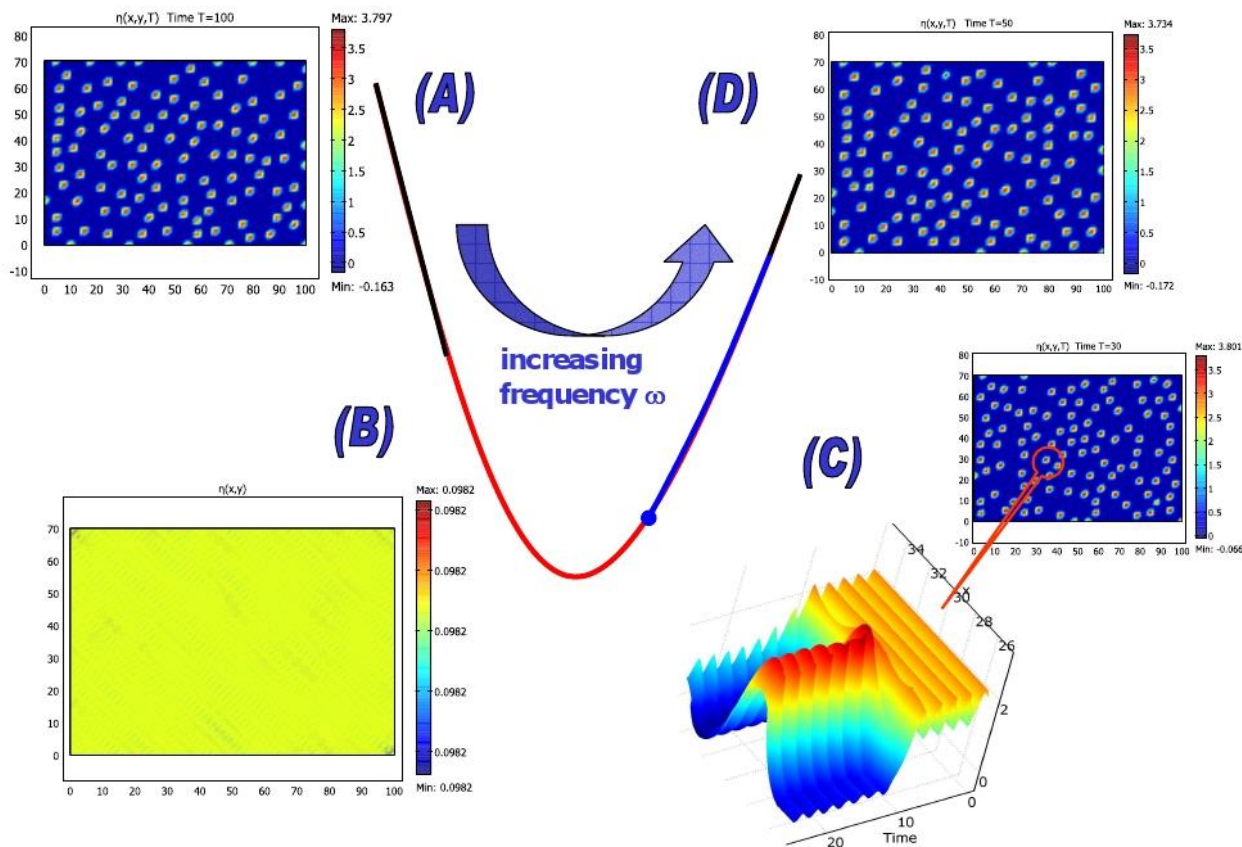


**Figure 1.** Dependence of morphology on frequency. Numerical simulations of the asymptotic morphologies  $\eta(x, y, T)$  at the final integration time T. For increasing values of the forcing frequency  $\omega$  (adimensional)( $\omega_{exp} [Hz] = \omega/100sec$ ), the four scenarios (A)--(D) are shown corresponding to distinct frequency ranges. To highlight the pulsating behaviour in the scenario (C), also the time evolution along an horizontal section starting from a flat initial condition towards an isolated spot is depicted. The numerical values of the frequency ranges are given by:  $[0, 10^{-3}]$  case (A);  $]10^{-3}, 2.57]$  case (B);  $]2.57, 50]$  case (C) and  $]50, 10^5]$  case (D).

Hence, for purposes of comparisons especially in the transient regions, we postprocess the numerical solutions obtained for the morphology  $\eta(x, y, T)$ ,  $(x, y) \in \Omega$  and  $t \in [0, T]$  to estimate the time behaviour of its mean value defined as  $\langle \eta(t) \rangle = \frac{1}{|\Omega|} \int_{\Omega} \eta(x, y, T) dx dy$ .

To outline the transient behaviours, corresponding to the four asymptotic scenarios listed above, in Fig.2 we report the time evolution of  $\langle \eta(t) \rangle$  from the perturbed unstable equilibrium to the stable one. In such time evolution, a well defined transient time  $t_{TR}$  can be identified in all cases.

From the plots reported in Fig. 2, for different frequencies  $\omega$ , it can be noted that  $t_{TR} = t_{TR}(\omega)$  exhibits a minimum value that corresponds to homogeneous morphology (see Fig. 1B).

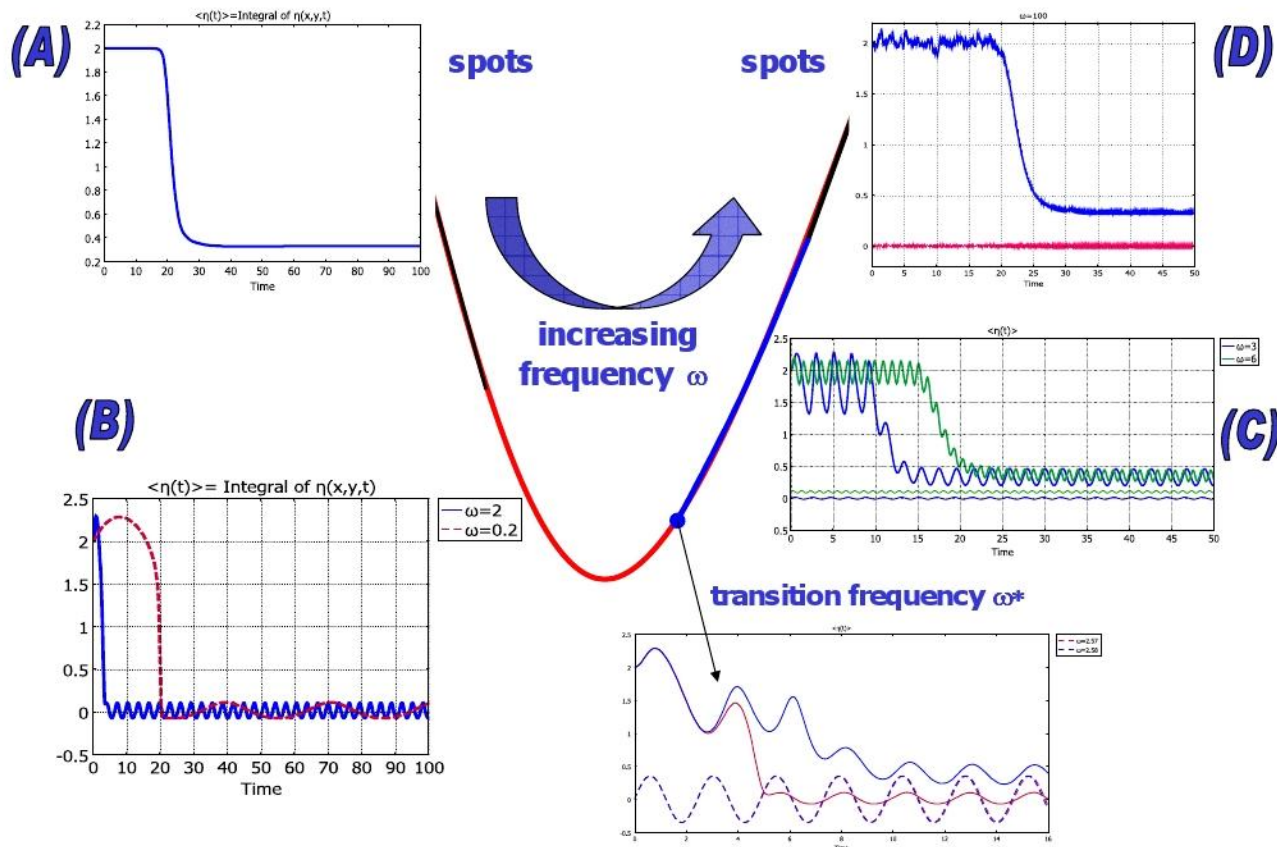


**Figure 2.** Insights on time evolution of morphology. Numerical simulations of the time evolution of the mean value of morphology  $\langle \eta(t) \rangle$  corresponding to representative values of the forcing frequency  $\omega$  (adimensional) in the four scenarios (A)–(D). Between panels (B) and (C) we show a plot pinpointing the effects of the existence of a critical frequency  $\omega^* = 2.57$  (red line,  $\omega = 2.58$  blue line) for the transition between morphologies (B) (homogeneous), and (C) (spots). In case (B) plots are shown for  $\omega = 0.2$ ,  $\omega = 2$ , in case (C) plots are shown for  $\omega = 3$  and  $\omega = 6$ . The numerical values of the frequency ranges are given by:  $[0, 10^{-3}]$  case (A);  $]10^{-3}, 2.57]$  case (B);  $]2.57, 50]$  case (C) and  $]50, 10^5]$  case (D).

- In scenario (A), there is a relatively fast transient, after which the spotty asymptotic surface is rapidly attained. In fact, the function  $\langle \eta(t) \rangle$  reaches a constant steady state in a comparatively short (adimensional) time, with respect to the other transients found in this study.
- In scenario (B), the numerical solution initially moves towards the spatially homogeneous equilibrium  $\eta_3^+$ , but soon the solution leaves it, eventually attaining an oscillating behaviour between two quasi-homogeneous surfaces, corresponding to the stable equilibria  $\eta_1^-$  and  $\eta_1^+$ .

- In scenario (C), during the transient, the solution oscillates around the starting value and then, for a critical time  $t^*$ , a spotty pattern develops, in which the spots pulsate with the forcing frequency, giving rise to a frequency-locking phenomenon. It is worth noting that the transition from the smooth patterns, characteristic feature of scenario (B), to the beat patterns typical of (C), takes place for a critical frequency  $\omega^*$ . Moreover, we also note that the critical time  $t^* = t_{TR}(\omega^*)$  for this transition, corresponds to that time when the phase difference between the frequency-locked process and the forcing term becomes significant (See Fig. 2C). We note that smooth morphologies are found when the forcing and the response are in phase, while dephasing correlates with unstable growth.
- Scenario (D) can be understood as a limiting case of scenario (C). In fact - as far as the pulsating behaviour is concerned - for highest frequencies investigated in this work, the pulsating spots exhibit such a fast beat and a small amplitude that they appear constant in time.

## 4. EXPERIMENTAL VALIDATION OF THE MODEL

### 4.1 Methods and materials

Our modelling work is systematically accompanied by experimental studies of metal-plating dynamics. In particular, we concentrated on some prototypical cases of Au - and Au-alloy electrodeposition [3—6].

We considered three types of cyanide-based baths for the electrodeposition of 18 and 24 kt Au-alloys: (i) AuCu, more suitable for red gold and Hamilton decorative finishes, (ii) AuCuCd, a typical electroforming bath and (iii) neutral  $\text{KAu}(\text{CN})_2$  solutions without added free cyanide: still a cyanide-based chemistry, but representing a notable step forward in terms of safety, with respect to free cyanide based chemistries. These baths consist in a metal source, in this case cyanide salts of the three relevant metals and two types of additives: (i) free complexing agent ( $\text{CN}^-$ , EDTA), typically used to extend the bath life, that can be jeopardised by loss of the complexing agent by environmental oxidation and (ii) organic levellers, in our case cetylpyridinium chloride (CPC) and benzyl-phenyl polyethylene imine (BPPEI) (for details, see [19]).

The composition and operating conditions of the alloy electrodeposition baths are reported below. (i) *AuCu bath*:  $\text{Au}^+$  (as  $\text{KAu}(\text{CN})_2$ )  $7.5 \text{ g L}^{-1}$ ,  $\text{Cu}^{2+}$  (as  $\text{CuO}$ )  $2.5 \text{ g L}^{-1}$ , EDTA  $11.5 \text{ g L}^{-1}$ , citric acid  $40 \text{ g L}^{-1}$ , ammonium citrate  $40 \text{ g L}^{-1}$ , pH 6, room temperature, current density  $20 \text{ mA cm}^{-2}$ . As a leveller we added CPC 100 ppm. (ii) *AuCuCd bath*:  $\text{Au}^+$  (as  $\text{KAu}(\text{CN})_2$ ),  $2.5 \text{ g L}^{-1}$ ,  $\text{Cu}^+$  (as  $\text{K}_2\text{Cu}(\text{CN})_3$ )  $60 \text{ g L}^{-1}$ ,  $\text{Cd}^{2+}$  (as  $\text{KCd}(\text{CN})_3$ )  $2.5 \text{ g L}^{-1}$ , pH 11,  $T=70^\circ\text{C}$ , current density  $10 \text{ mA cm}^{-2}$ . (iii)  $\text{KAu}(\text{CN})_2$  10 mM,  $\text{NaClO}_4$  0.1M, pH 7.

In the case of the free cyanide bath, KCN  $25 \text{ g L}^{-1}$  was added. As a leveller we added 10 ppm of BPPEI.

These two additives have two chief types of effect on interfacial electrochemistry. Cyanide is strongly adsorbed at the growing surface, thus affecting adatom diffusivity (see, e.g. [20]). In terms of our model, higher  $\text{CN}^-$  concentrations in the bath give rise to a reduction of  $D_{sc}^*$ , that - if  $D_s^* \approx \text{const}$  - of course implies a reduction of  $d$ . The leveller typically forms an interfacial organic film between

the metallic surface and the aqueous electrolyte, generally (some exceptions are related to the existence of resonance tunneling processes [21] providing an additional barrier - with respect to a compact layer of water - to electron tunneling from the metal to the electroactive metal cation. Within the framework of quantum chemical kinetics, this can be viewed as a decrease of the phenomenological electrokinetic parameter  $a$ .

Both parameters  $d$  and  $a$  are relevant for the presence of morphological patterns, as explained in the Section 2.

#### 4.2 Microscopy and roughness measurements

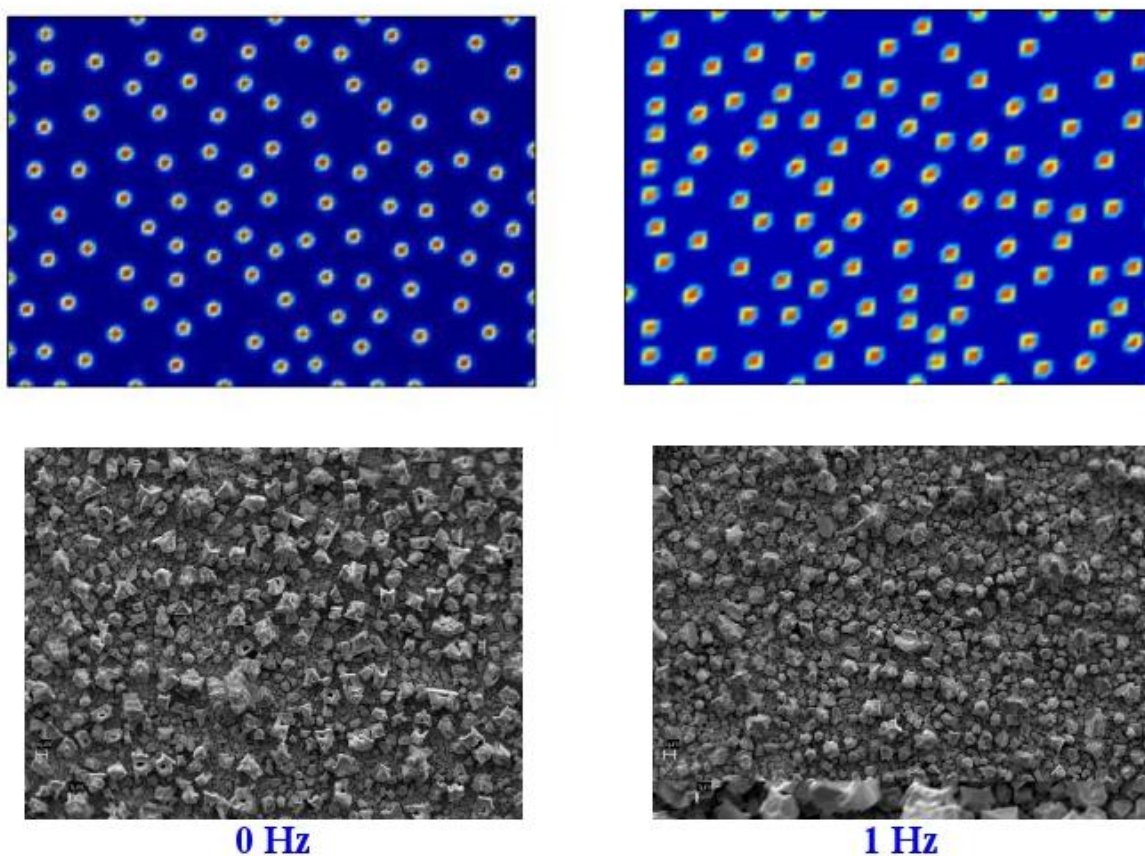


**Figure 3.** Experimental validation of the model. Top row: numerical simulations of the asymptotic morphologies  $\eta(x, y, T)$  at the final integration time  $T$  corresponding to the unforced model (left panel) and to the model with forcing frequency  $\omega \in ]0, 10^{-3}]$  corresponding to the scenario (A) (right panel). Bottom row: SEM micrographs of Au electrodeposits obtained potentiostatically with a bias of  $-1.6\text{V}$  vs.  $\text{Ag}/\text{AgCl}$  without (left panel) and with added sinusoid of frequency  $1\text{Hz}$  and amplitude  $0.01\text{V}$  (right panel) (deposition time: 30 min; for further chemical and electrochemical details, see Section 4).

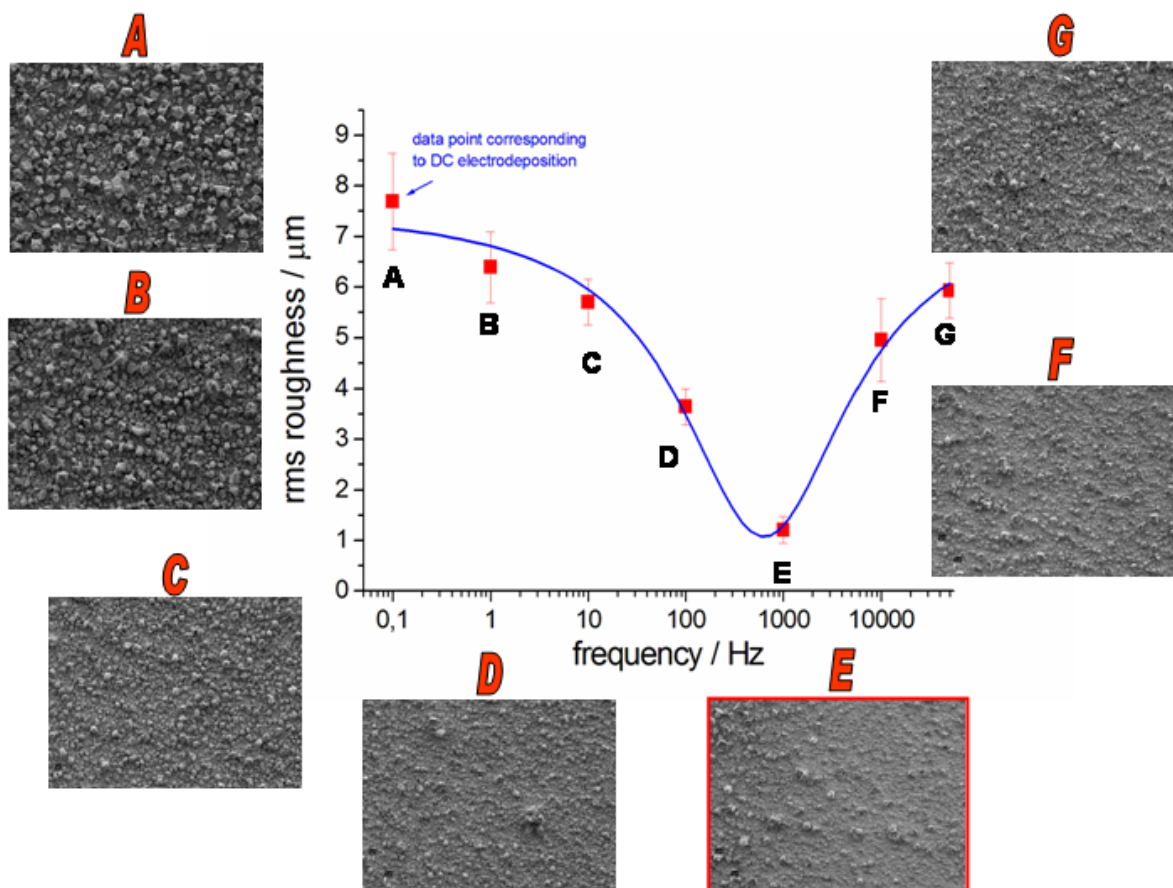


**Figure 4.** Electrodeposit roughness as function of frequency. SEM micrographs of Au electrodeposits obtained potentiostatically with a bias of  $-1.6\text{V}$  vs. Ag/AgCl with added sinusoid of amplitude  $0.01\text{V}$  and corresponding *rms* roughness estimates obtained by laser interferometry. Frequencies in Hz are shown in the abscissae of the *rms* roughness function. (deposition time: 30 min). For further electrochemical details, see Section 4.

In order to assess the effects of frequency on the morphology of electrodeposits, we used a classical electroplating system, well known from the literature (see, e.g. [22] and references therein contained) and insightfully investigated in our group: electrodeposition of Au from a neutral  $\text{KAu}(\text{CN})_2$  solution without additives. This system exhibits largely suboptimal properties in terms of deposit quality - especially as far as roughness is concerned - and can be regarded as a benchmark for levelling efficiency. In this research we carried out electrodeposition with a cathodic bias of  $-1.6\text{V}$  vs. Ag/AgCl - that has been proved to give rise to typical unstable growth morphologies [23] - to which a sine wave of amplitude  $0.01\text{V}$  has been added, of frequencies in the range  $0 \div 50\text{ kHz}$ . SEM micrographs of the corresponding Au deposits are shown in Figs. 3 and 4 - corresponding to electrodeposition for 30 min - as well as in Fig. 5, showing the surface of films grown under otherwise identical conditions for 2 hours.

From Fig. 3 one can conclude that the application of low frequencies does not essentially change the deposit morphology with respect to conventional potentiostatic conditions that, with the

relevant electroplating parameters, yield an unstable growth morphology of the type (A), that is spots [5]. Numerical simulations corresponding to these conditions are also shown in the same figure.

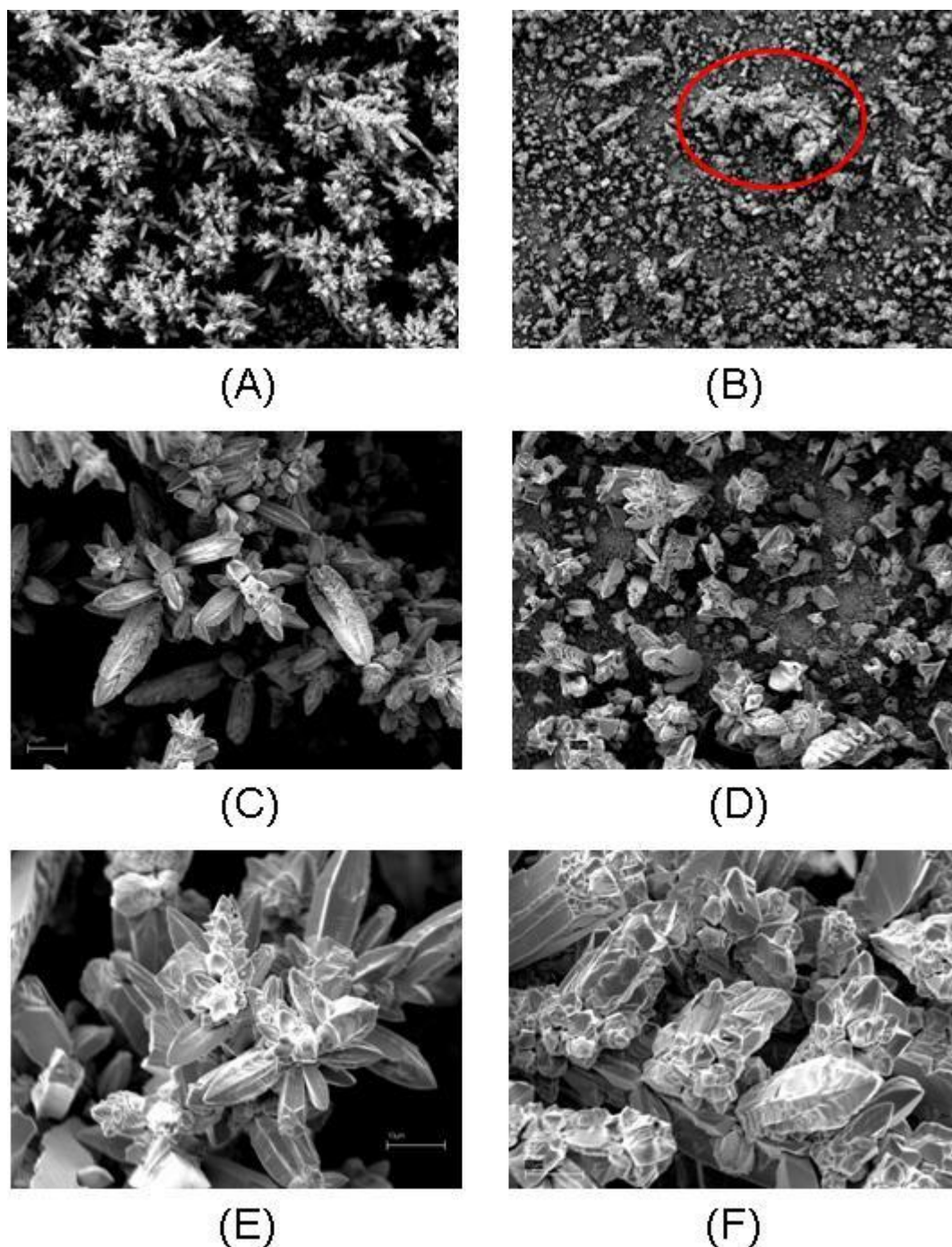


**Figure 5. Frequency effect on Au electrodeposition.** SEM micrographs of Au electrodeposits: bias - 1.6 V vs. Ag/AgCl, deposition time: 2 hours; sine amplitude: 0.01V. Frequencies: 0 Hz, in panels (A, C, E) and 500 Hz in panels (B, D, F). Magnifications are : 100 x in panels (A, B), 500 x in panels (C, D) and 1500 x in panels (E, F). Micrographs in (D) and (F) are enlargements of the area highlighted in (B).

Fig. 4 shows that there exists a range of frequencies - centered at a few hundred Hz - where, under otherwise identical conditions, a smoothing effect is obtained. Instead, at the highest frequencies investigated - in the range of some tens of kHz - the smoothing effect is no longer present and the morphology is again essentially the same as with DC plating.

These experimental results are consistent with the asymptotic computations reported in Fig.1, predicting the existence of an intermediate frequency range (scenario (B)) where more homogeneous morphologies develop. It is also worth noting that our transient computations (see Fig. 2) have shown that such a critical frequency range also give rise to a special dynamic behaviour, leading to fast relaxation from the unstable equilibrium to the stable one.

Three-dimensional surface roughness data were acquired with a Rodenstock RM-600 optical setup with non-contact laser interferometric transducer - based on [24] -, by means of a dynamically focussed infrared laser with a 2m focal point. The Rodenstock readings were digitised and the raw data elaborated with suitable routines developed by us. The most significant roughness estimator can be proved to be the *rms* (root mean square) roughness, in the case of electrodeposits [24,25].

These results has been further confirmed by plating for a longer time in DC conditions and with a superimposed sinewave of 500Hz: the corresponding micrographs are shown in Fig. 5 highlighting the stabilising effects of frequency within the smoothing range.

As far as the experimental confirmation of scenarios (B) and (C) are concerned, it is worth noting that it seems not currently possible to detect the oscillating planes and the frequency-locking process found numerically. In fact, essentially all electrochemical microscopies are sensitive to time-integrated morphological dynamics. Instantaneous morphological changes can be tracked by in situ electrochemical STM, but it does not seem possible to perform this type of investigation in the case of 3D growth morphologies. In principle, it would be possible to image by STM a location of a given 3D feature and follow its evolution, but present-day fast-scanning devices would be unable to track morphological fluctuations at the frequency required in this study. Recent advances in X-ray microscopy exhibit some capability of dynamic 3D imaging [26], but the currently achievable image acquisition rate, even in the case of synchrotron-base techniques, is insufficient for the present case. Indirect methods, such as the tracking of optical enhancing effects by in situ spectroelectrochemical methods, currently lack the required lateral resolution for an appropriate microscopy [23]. Tip-enhanced versions of these approaches are still in their infancy and, in principle, would exhibit the same drawbacks as in situ STM.

## 5. CONCLUSIONS

In this research we have shown that smoothing effects can be achieved in potentiostatic metal electroplating processes if a small-amplitude (ca. 10mV) potential sinusoid - of frequency contained in an appropriate range (a few hundred Hz) - is summed to the applied DC bias. Similar smoothing effects are obtained in the industrial practice with the addition of toxic chemicals to the process solutions. On the basis of mathematical modelling, this effect has been explained in terms of the

coupling between the dynamics of processes controlling the time evolution of metal morphology and interfacial chemistry.

Nonlinear dynamical system theory and numerical simulations have been used to explore the effect of a periodic external forcing on the Turing patterns found in the unforced case, focussing on the influence of the periodic driving force in pattern suppression. We discussed the interesting mathematical aspects of (i) morphological *asymptotic* scenarios and (ii) morphological *transient* behaviours. The mathematical work is complemented by the experimental validation of the modelling predictions for the case of Au electrodeposition. Our results show that an insightful understanding of the dynamics of reacting systems can offer green solutions to problems that are traditionally attacked with the use of non-sustainable chemistries.

## References

1. D. Thiemig, A. Bund, J.B. Talbot, *Electrochim. Acta*, 54 (2009) 2491
2. B. Bozzini, I. Sgura and L. D'Urzo, in: A. El Nemr Eds., *New Developments in Electrodeposition and Pitting Research*, Research Signpost Pub., Fort P.O, Trivandrum-695 023, Kerala, India, 2007, 11
3. B. Bozzini, D. Lacitignola and I. Sgura, *J. of Physics: Conf. Series* 96, (2008), 012051
4. B. Bozzini, D. Lacitignola, I. Sgura, *Math Comput. Simul.*, 81, N.5 (2011) 1027
5. B. Bozzini, D. Lacitignola, I. Sgura, *Math. Biosc. and Engin.* 7, N. 2, (2010) 237
6. B. Bozzini, D. Lacitignola, I. Sgura, C. Mele, M. Marchitto, A. Ciliberto, *Adv. Materials Res., Trans Tech Pubs* 138 (2010) 93, doi:10.4028/www.scientific.net/AMR.138.93
7. A.Pimpinelli, J. Villain, *Physics of Crystal Growth*, Cambridge University Press, Cambridge (1998)
8. J. Villain, *J. Phys. I France*, 1 (1991) 19
9. E. Gileadi, *Electrode Kinetics for Chemists, Chemical Engineers and Materials Scientists*, Wiley-VCH Verlag, New York (1993)
10. J. Goodisman, *Electrochemistry: Theoretical Foundations*, J. Wiley & Sons (1987)
11. R. Kapral, K. Showalter, *Chemical Waves and Patterns*, Kluwer Academic Publishers (1995)
12. T. K. Callahan, E. Knobloch, *Physica D*, 132 (1999) 339
13. J. D. Crawford, *Rev. Mod. Phys.* (1991) 63
14. G. Dewel, P. Borckmans, A.D. Wit, B. Rudovics, J. Perraud, E. Dulos, J. Boissonade and P.D. Kepper, *Physica A* 213 (1995) 181
15. A.C. Newell, T. Passot and J. Lega, *Ann. Rev. Fluid Mech.* 25 (1993) 399
16. K.I. Popov, S.S. Djokic and B.N. Grgur. *Fundamental Aspects of Electrometallurgy*, Kluwer, New York (2002)
17. R. Winand, *Hydrometallurgy* 29 (1992) 567
18. COMSOL MULTIPHYSICS v.3.5 User's guide (2008)
19. B. Bozzini, L. D'Urzo and C. Mele, *Electrochim. Acta*, 52 (2007) 4767
20. B. Bozzini, A. Fanigliulo, *J. Cryst. Growth* 243 (2002) 190
21. E.E. Farndon, F.C. Walsh and S.A. Campbell, *J. Appl. Electrochem.* 25 (1995) 574
22. B. Bozzini, L. D'Urzo, C. Mele, V. Romanello, *J. Phys. Chem. C*, 112 (2008) 6352
23. B. Bozzini, L. D'Urzo, D. Lacitignola, C. Mele, I. Sgura, E. Tondo, *Trans. of The Institute of Metal Finishing*, 87, No 4 (2009) 193
24. R. Brodmann, Th. Gast, G. Thurn, A. Wirtz and Optische Werke G. Rodenstock, *CIRP Annals - Manufacturing Technology*, 33 (1984) 403
25. B. Bozzini, *Il Vuoto*, 26 (1997) 18

26. B. Bozzini, L. D'Urzo, A. Gianoncelli, B. Kaulich, M. Prasciolu, I. Sgura, E. Tondo, M. Kiskinova, *J. of Phys. Chem C*, 113, No 22 (2009) 9783
27. B. Bozzini, G. Giovannelli and P.L. Cavallotti, *J. Appl. Electrochem.* 29 (1999) 685
28. B. Bozzini, P.L. Cavallotti and G. Giovannelli, *Met. Fin.* 100 (2002) 50
29. Krischer K. In: B.E. Conway, J.O. Bockris and R. White, Eds, *Modern Aspects of Electrochemistry*, Plenum, New York (1999)
30. J.L. Hudson, T.T. Tsotis, *Chem. Eng. Sci.* 49 (1994) 1493
31. B. Bozzini, G. Giovannelli and C. Mele, *Surf. & Coat. Technol.* 201 (2007) 4619

## APPENDIX

### *Continuous modeling of electrodeposition dynamics: motivation and mathematical details*

In the electrochemical context, electrodeposition of Au alloys from cyanocomplex baths has been shown to exhibit electrokinetic instabilities that can lead to compositional heterogeneity in the electrodeposit bulk [27]. Such instabilities typically derive from hysteretic current-voltage characteristics, related to the buildup of  $\text{CN}^-$  concentration in the catholyte and attending variations of surface coverage with adsorbed  $\text{CN}^-$  as well as to cyanocomplex nobility [28]. This phenomenon is a special case, original within the realm of metal electrochemistry, of a more general, well-known type of chemical and electrochemical dynamics (electrocatalysis [29], corrosion of *Cu* [30], *Fe*-group metals [29] and *Ag* [31]).

In the past, we considered a reaction-diffusion approach to model metal growth processes within the electrodeposition context (ECD), focussing on morphological pattern formation in a finite two-dimensional spatial domain [2--5]. Thus we developed a model coupling the surface morphology and additive surface concentration.

In [5] the nonlinear dynamics of the system was studied both theoretically and numerically and the problem of diffusion-driven pattern formation and pattern selection was addressed. System analysis has revealed the crucial role of specific parameters for stability and selection of solutions. We obtained a set of conditions – in terms of the system parameters - ensuring the initiation of spatial pattern induced by diffusion. To this aim - according to its chemical meaning - the diffusion parameter  $d$  was shown to be essential for the arising of instability and the appearance of spatial patterns. Our previous studies also revealed the peculiar role in tuning pattern selection, played by the parameter  $a$  - representing the inverse of the barrier that has to be overcome by electrons tunneling from the electrode into the electrolyte to reduce metal adatom precursors (e.g. [10]). Fixing  $d \approx d_c$  where  $d_c$  is the threshold value of diffusion in order to produce diffusion-driven spatial pattern initiation -, we have found that lower values of the parameter  $a$  caused a coexistence between different pattern types, i.e. spotty and worm-like patterns, whereas higher values of the parameter  $a$  resulted only in spotty patterns.

We found that such a phenomenology is in close agreement with experimental physico-chemical evidence.

As mentioned in the main text of this paper, Continuous Modelling (CM) of crystalline film growth can be regarded as an acceptable description of profile dynamics, provided the following

conditions on length- and timescales are met. If a crystal is made to grow some way, in particular by electrodeposition, steps are present on its surface, either because they are implied by the preparation conditions - in which case they play the role of an initial condition -, or because they form in nucleation events occurring during the growth process itself. If  $l_s$  is the average distance between steps, CMs are suitable to study morphological features that are  $\gg l_s$ . Studying features with typical lengthscales  $\gg l_s$ , implies that mechanisms are operative, able to heal the surface on a distance  $l_s$ , in the relevant case, chiefly surface diffusion. This means that the morphologies that are going to be considered - in particular, the roughness as measured e.g. in terms of statistical estimators - derive from the averaging of several random processes, such as source intensity, sticking, diffusion and nucleation of rate of formation of new crystal terraces. In practice, even though different models are more appropriate for other - tendentially subnanometric or atomic - lengthscales, CMs are found to give a simple theoretical description of crystal growth on the mesoscopic scale (say  $nm$  to several tens of  $m$ ) and in general beyond ca. 50 atomic distances [8].

As far as the timescale is concerned, CM is a suitable dynamic description for times longer than those necessary to complete an atomic layer. In addition, it is a common assumption that temperatures are low enough not to bring about thermal smoothing of the surface: this is a very reasonable hypothesis in the case of electrochemical growth.

### A.1 Conditions for diffusion-driven pattern formation in the unforced model

The mathematical model proposed in this paper to study the dynamics of the morphology  $\eta(x, y, t)$  and of the chemistry  $\theta(x, y, t)$  in presence of a forcing voltage is the reaction-diffusion PDE system in Eq. (3) of the main text. In the first equation, the source term for the morphology evolution is

$$f(\eta, \theta) = \frac{\varepsilon \eta^2}{1 + \eta} - \eta \theta, \tag{8}$$

$$F(t) = \tilde{A} \sin(\sigma \omega t) \tag{9}$$

where  $F(t)$  corresponds to the forcing voltage of (adimensional) amplitude  $\tilde{A} = K A_0$ . The parameter  $K = 2i_0 \times a \times n$  (see Eq. (6) of main text), assembles the electrokinetic Butler-Volmer parameters ( $[K] = 1/V$ ) and  $A_0[V]$  is the amplitude of the imposed sinusoid.

In the second equation for the chemistry, the reaction term is given by

$$g(\eta, \theta) = K_{ADS}^*(\eta, \theta)(1 - \theta) - K_{DES}^*(\eta, \theta)\theta, \tag{10}$$

$$K_{ADS}^* = A \exp(a\eta + b\theta), \quad K_{DES}^* = A_1 \cdot \exp(a_1\eta + b_1\theta) \tag{11}$$

On the basis of very reasonable physico-chemical assumptions, we reduced the dimensionality of the parameter space of the reaction-diffusion model by considering the following constraints on the system parameters:

$$A \neq A_1, \quad a \neq a_1 \quad b = b_1 \quad a_1 = a + \varepsilon \ln\left(\frac{A}{\varepsilon A_1}\right) \quad \frac{A}{A_1} = \frac{\varepsilon}{2}.$$

As a consequence, the reaction term (10)-(11) specializes as:

$$g(\eta, \theta) = \frac{A}{\varepsilon} \exp(a\eta + b\theta) (\varepsilon(1 - \theta) - \theta 2^{1-\varepsilon\eta}), \tag{12}$$

An extensive presentation of this subject matter is available in [2, 3, 5] with regard to the *unforced model* ( $F(t) \equiv 0$ ). In this case, as comprehensively exposed in [5], the spatially uniform steady state  $E_2 = (\eta_2, \theta_2) = \left(\frac{1}{\varepsilon}, \frac{\varepsilon}{\varepsilon + 1}\right)$  may undergo diffusion-driven instability. Initiation of spatial patterns induced by diffusion is shown to occur in a suitable region of the parameter space, defined by the following set of conditions:

$$\left\{ \begin{array}{l} \rho\varepsilon^3 - A\sigma\gamma(\varepsilon + 1)^3 < 0 \\ A\sigma\gamma(\ln 2 - \varepsilon) > 0 \\ d\rho\varepsilon^3 - A\sigma\gamma(\varepsilon + 1)^3 > 0 \\ \left[ \frac{d\rho\varepsilon^3 - A\sigma\gamma(\varepsilon + 1)^3}{\varepsilon(\varepsilon + 1)^2} \right]^2 - \frac{4d\rho}{\varepsilon + 1} A\sigma\gamma(\ln 2 - \varepsilon) > 0 \end{array} \right. \tag{13}$$

where  $\gamma = \exp(\alpha_0)$ ,  $\alpha_0 = \frac{a}{\varepsilon} + \frac{b\varepsilon}{\varepsilon + 1}$ .

These inequalities allow us to locate a region in the parameter space such that  $E_2$  is stable to small perturbations in the absence of diffusion, but it can be unstable to small spatial perturbations when the diffusion parameter  $d$  is non-zero and greater than a critical value  $d_c$ . When the other parameters are fixed,  $d_c$  can be determined by combining the third and fourth conditions in the set of inequalities (13).

For example, fixing  $\varepsilon = 0.5, \rho = 40, \sigma = 2, a = 1, b = 1$  and considering  $A$  and  $d$  as bifurcation parameters, it is easy to show that conditions (13) are verified for  $A > A_c = 0.07183$  and for  $d$  verifying:

$$d > 13.92A, \quad \varphi_2 d^2 - \varphi_1 A d + \varphi_0 A^2 > 0, \tag{14}$$

where  $\varphi_2=4.93827$ ,  $\varphi_1=243.72524$ ,  $\varphi_0=957.08407$ . Hence, by choosing the parameter  $A$  so that  $A=0.2 > A_c$ , for spatial patterns to arise, the diffusion parameter  $d$  has to be greater than  $d_c=9.1$ .

The physical meaning of the choice of specific sets of numerical values has been thoroughly discussed in [2, 3, 5].

Numerical results in [5], have been obtained by fixing the parameters of the system such that:

$$\varepsilon = 0.5, \rho = 40, \sigma = 2, b = 1, A = 0.2, d = 10 \quad (15)$$

and varying  $a$  in order to outline its role in pattern selection. The motivation for this choice is based on both structural and experimental evidence. In order to verify conditions (13),  $a$  must vary in the range  $a \in [a_{\min}, a_{\max}]$ , where, for the chosen parameter values,  $a_{\min}=0.4879$  and  $a_{\max}=1.05209$ .

Under the physico-chemical approximations adopted to write the model (and in particular as far as the source term for the morphology equation (3)<sub>1</sub> is concerned), the variable  $\eta$  - having primarily the meaning of dimensionless morphology - is essentially proportional to the local overvoltage, driving the electrodeposition process out of equilibrium.

According to the physical meaning of the parameter  $a$ , low values of  $a$  correspond to inhibited electron tunneling resulting in a lower rate of adatom formation, eventually giving rise to a lower surface concentration of adatoms that have a better chance to diffuse to low-energy sites, giving rise to a more stable morphology, exhibiting less singularities. From the experimental point of view, lower  $a$  values can be obtained by adding special chemicals to the electrodeposition solutions: more physico-chemical details and experimental results are reported in [5]. High values of  $a$  corresponding to higher growth rates are related to more unstable morphologies (see, e.g. [16, 19]).